UNIVERSIDAD AUTÓNOMA DE SINALOA
FACULTAD DE CIENCIAS DE LA TIERRA Y EL ESPACIO

Observatorio Infotecnológico de las Ciencias de la Tierra y el Espacio

BOLETÍN VOL. 8, NÚM. 1
ENERO 2020

CONTÁCTANOS EN:

observatorio.facite@uas.edu.mx

PÁGINA WEB:

http://facite.uas.edu.mx/observatorio/

UNIVERSIDAD AUTÓNOMA DE SINALOA
FACULTAD DE CIENCIAS DE LA TIERRA Y EL ESPACIO

Observatorio Infotecnológico de las Ciencias de la Tierra y el Espacio

Boletín Vol. 8, Núm. 1
Enero 2020

Contenido

Directorio

UNIVERSIDAD AUTÓNOMA DE SINALOA
FACULTAD DE CIENCIAS DE LA TIERRA Y EL ESPACIO

ARTÍCULOS: GEODESIA, GEOMÁTICA Y ASTRONOMÍA

Characterization of rain impact on L-Band GNSS-R ocean surface measurements

Balasubramaniam, R. and Ruf, C., (2020). *Remote Sensing of Enviroment,* 239.

Abstract

Earth remote sensing using reflected GNSS signals is currently an emerging trend especially in ocean surface-wind measurements. Unlike the existing scatterometer missions, GNSS-R uses L-Band navigation signals that can penetrate through clouds and rain. Rain may have a negligible impact on the transmitted signal in terms of path attenuation at this wavelength. However, there are other effects due to rain, such as changes in Surface roughness and rain induced local winds, which can significantly alter the measurements. Currently, there is no observation-based characterization of all possible impacts of rain on radar forward scatter, which is the nature of operation of GNSS-R missions. In this study, we propose a 3-fold rain model which accounts for attenuation, surface effects of rain and rain induced local winds. We utilize the large dataset of measurements made by theCYGNSS mission to separate these different effects of rain. The attenuation model suggests that a total of at least 96% transmissivity exists at L-Band up to a rain rate of 30 mm/h. A perturbation model is used to characterize the other rain effects. It suggests that rain is accompanied by an overall reduction in the scattering cross-section of the ocean surface and, most importantly, this effect is observed only up to surface wind speeds of 15 m/s, beyond which the gravity capillary waves dominate the scattering in the quasi-specular direction. Observations also suggest that, at very low wind speeds, the lower bound on wavenumber of the portion of the Surface roughness spectrum that influences the measurements deviates from the geometric optics approximation normally used. This work binds together several rain-related phenomena and enhances our overall understanding of rain effects on GNSS-R measurements.

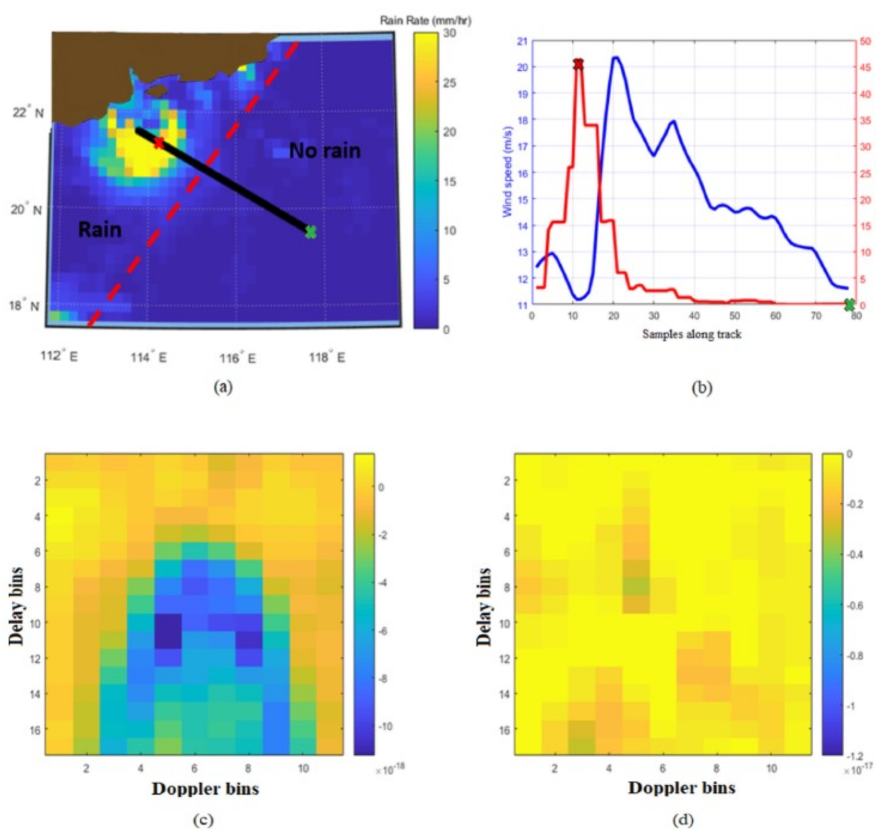

Figure 1. GEBCO bathymetry and topography of the study area with GPS sites from IGS and Japanese GEONET networks. The red star represents the epicentre of Mw9.0 Tohoku-Oki earthquake on11th March, 2011 at central Japan. The concentric circles represent various radial distances defined from the epicentre.

Recuperado de: https://doi.org/10.1016/j.rse.2019.111607

UNIVERSIDAD AUTÓNOMA DE SINALOA
FACULTAD DE CIENCIAS DE LA TIERRA Y EL ESPACIO

Migration of shallow and deep slow earthquakes toward the locked segment of the Nankai megathrust

Uchida, N., Takagi, R., Asano, Y., Obara, K., (2020) *Earth and Planetary Science Letters,* 531.

Abstract

The Nankai megathrust is located offshore Shikoku and Kyushu, Japan and is characterized by various kinds of slow earthquakes whose relative motions across the plate boundary faults are slower than regular earthquakes. In the area, the interplate locking is stronger in the northern area (offshore Shikoku) than in the southern area (offshore Kyushu) and Mw □8 earthquakes (Nankai earthquakes) have occurred repeatedly in the northern area. In this paper, the spatio-temporal distributions of slow earthquakes (very low frequency earthquakes, tremors and slow-slip events) are examined based on the analyses of repeating earthquakes and slow earthquakes with special focus on the interaction between different activities. A comprehensive analysis of the seismic and geodetic data from 2003 to 2016 indicates complementary distribution of various types of slow earthquakes down to 35–50 km depth outside the Nankai main locking area. We also found interactions between different kinds of activities. The interactions between the repeating earthquakes and slow earthquakes suggest that the area of the repeating earthquakes activity can be divided into deeper (depth ≥20km) and shallower (depth <20km) areas. The analyses of deep repeating earthquakes and the inland Global Navigation Satellite System (GNSS) data suggests slow northward migrations of long-term slow slip events (SSEs) in 20–50km (offshore Kyushu) and 20–35km (under Shikoku) depths along the plate boundary. These migrations occurred during a period of 2–3 years that includes the 2003 and 2010 large slow-slip events in the Bungo channel located in between Kyushu and Shikoku. The analysis has also shown interaction between shallow repeating earthquakes and shallow very low frequency earthquakes which indicates faster northward migrations of short-term SSEs from the shallow plate boundary offshore Kyushu to the deeper area under Shikoku over the duration of a month during the 2010 long-term slow-slip episode. The deep slow migration and the shallow to deep fast migration of SSEs in a ~300 km area towards and around the source area of the recurrent Nankai earthquake (Mw 8.0–8.6) indicates the occurrence of a widespread non-steady stress build-up process around the source area of the Nankai megathrust earthquake.

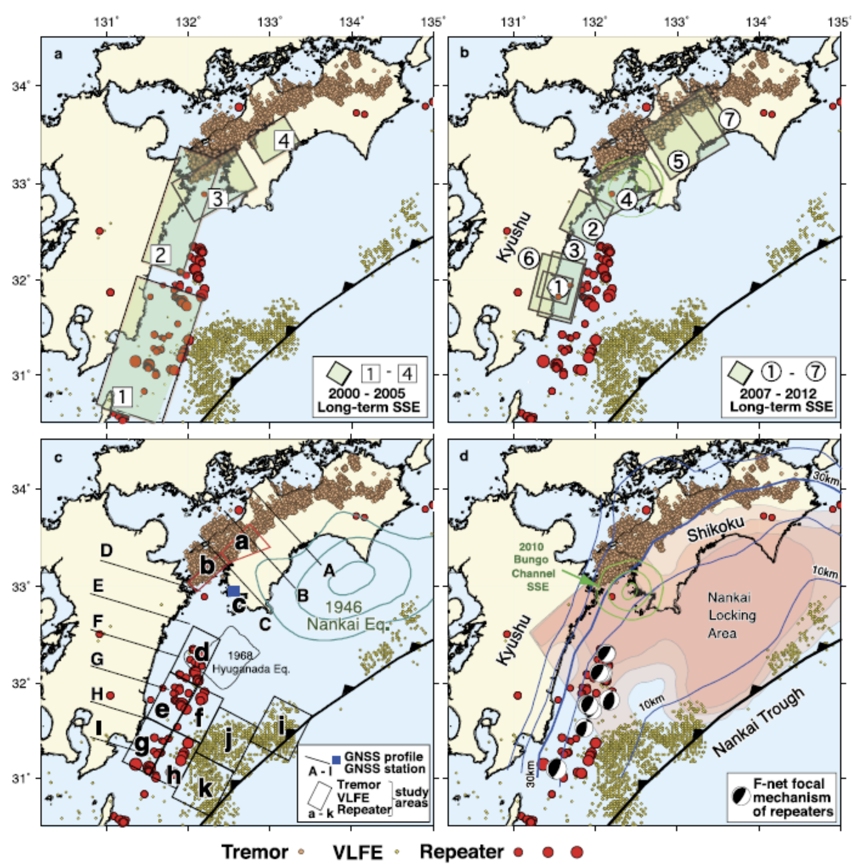

Figure 1. Distribution of non-volcanic tremors (orange circles), very low frequency earthquakes (yellow circles), and repeatingearthquakes (red circles) associated with (a) source areas of long-term SSEs (Takagi et al., 2019) from 2000 to 2005, (b) and from 2007 to 2012; (c) GNSS stacking profiles (from A to I), a GNSS station for the comparison with slow earthquakes(square c) and the study areas for tremor (regions a and b), VLFE (regions i to k), repeaters (regions d to h), and (d) F-net focal mechanisms of repeating earthquakes. In (c), the coseismic slip areas for the 1946 Mw 8.3 Nankai earthquake (Sagiya and Thatcher, 1999) (green contours, denoting 2, 5 and 10 m slips), and for the 1968 M7.5 Hyuga-nada earthquake (Yagi et al., 1998) (black contour) are also shown. In (d), pink shaded colors, green contour lines, and blue contour lines show the slip deficit rate of 3, 4, and 5 cm/year (Yokota et al., 2016), the slip distributions of the 2010 Bungo channel long-term SSE with 10 cm intervals (Geospatial Information Authority of Japan, 2014), and the geometry of the plate interface at 10 km intervals (Baba et al., 2002; Hirose et al., 2008).

Recuperado de: https://doi.org/10.1016/j.rse.2019.111607

UNIVERSIDAD AUTÓNOMA DE SINALOA
FACULTAD DE CIENCIAS DE LA TIERRA Y EL ESPACIO

Improving tropospheric corrections on large-scale Sentinel-1 interferograms using a machine learning approach for integration with GNSS-derived zenith total delay (ZTD)

Kearns, T., Wang, G., Turco, M., Welch, J., Tsibanos, V. and Liu, H., (2018). *Geodesy and Geodynamics,* 10, 382-393.

Abstract

Sentinel-1 mission with its wide spatial coverage (250 km), short revisit time (6 days), and rapid data dissemination opened new perspectives for large-scale interferometric synthetic aperture radar (InSAR) analysis. However, the spatiotemporal changes in troposphere limits the accuracy of InSAR measurements for operational deformation monitoring at a wide scale. Due to the coarse node spacing of the tropospheric models, like ERAInterim and other external data like Global Navigation Satellite System (GNSS), the interpolation techniques are not able to well replicate the localized and turbulent tropospheric effects. In this study, we propose a new technique based on machine learning (ML) Gaussian processes (GP) regression approach using the combination of small-baseline interferograms and GNSS derived zenith total delay (ZTD) values to mitigate phase delay caused by troposphere in interferometric observations. By applying the ML technique over 12 Sentinel-1 images acquired between May–October 2016 along a track over Norway, the root mean square error (RMSE) reduces on average by 83% compared to 50% reduction obtained by using ERA-Interim model.

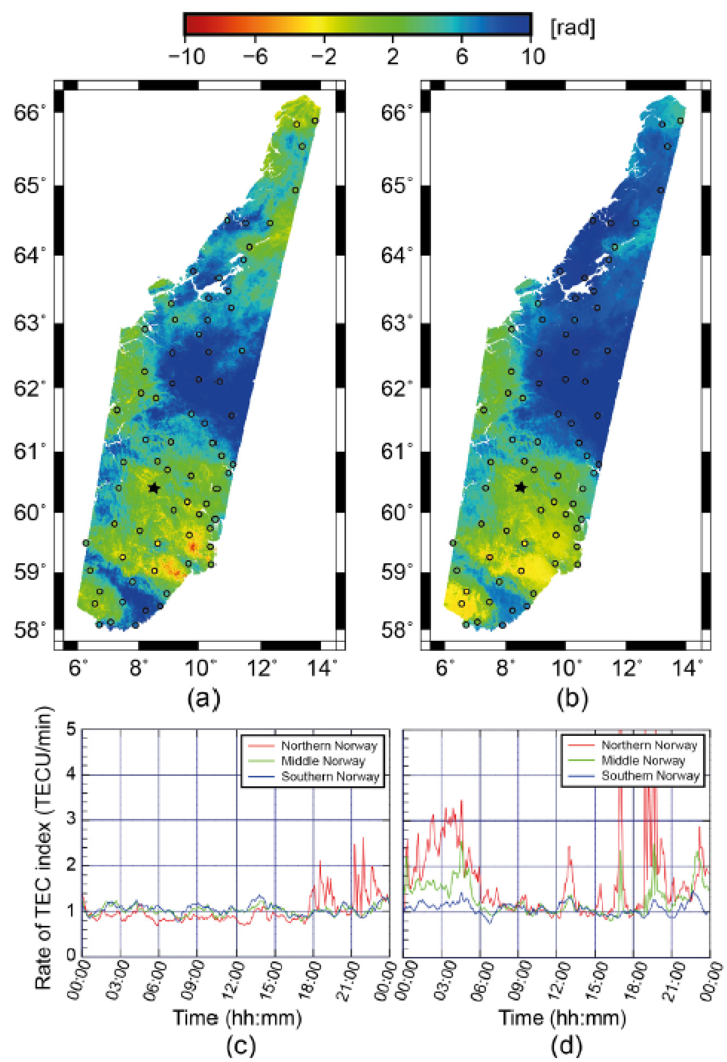

Figure 1. An example of tropospheric map from InSAR and GNSS-based method (using machine learning) on the interferogram “20160822–20160903”. (a) the original interferogram, and (b) the predicted differential STD map. (c and d) the mean rate of TEC index observed at ground location for northern, middle and southern Norway in the dates 20160822 and 20160903, respectively (Courtesy http://sesolstorm.kartverket.no). 0–1 TECU/min means the low activity, while 3–5 TECU/min means the high activity. The circles in (a and b) show the GNSS stations locations, color-coded by the interferometric phase and the differential STD values, respectively, used for the model training. The star in (a and b) shows the location of the reference area, which is one of the GNSS stations.

Recuperado de: https://doi.org/10.1016/j.rse.2019.111608

A GIS-based site investigation for nuclear power plants (NPPs) in Nigeria

Eluyemi, A., Sharma, S.m Olotu, S., Falebita, D., Adepelumi, A., Tubosun, I., Ibitoye, F and Baruah, S., (2020). *Scientific African,* 7.

Abstract

The Nigeria Atomic Energy Commission (NAEC) has identified some sites for possible con- structions of nuclear power plants in Nigeria. This paper addresses the conduct of a Ge- ographic Information System (GIS) based suitabi- lity assessment of these sites for the pro- posed Nuclear Power Plant. Attempts to recommend sites for the nuclear power plants and other major constructions in Nigeria have been made in view of historical and recent occurrences both at regional and local level, with earthquake occurren- ces in Ghana (18th December, 1636 M s = 5.7; 1862 M L ~6.5 and M s ≥6.5; 11th February, 1907 and 22nd of June, 1939 M s ~6.5 and m b ~6.4), Guinea 22nd December, 1983 with (M W ~6.3) coupled with recent activities of volcanic eruption of mount Cameroun (1986, 1999, 20 0 0). The buried equatorial fault lines emanating from the seismically active zones of the Gulf of Guinea are in reac- tivation state. This study entails the use of GIS to integrate available ad- ministrative and comprehensive tectonic maps of Nigeria. Database for the recommended sites is in line with the guidelines and recommendations of the Inter- national Atomic En- ergy Agency. In this paper, recom- mended sites are those where seismic and other hazards are considered to be at the bearest minimum.

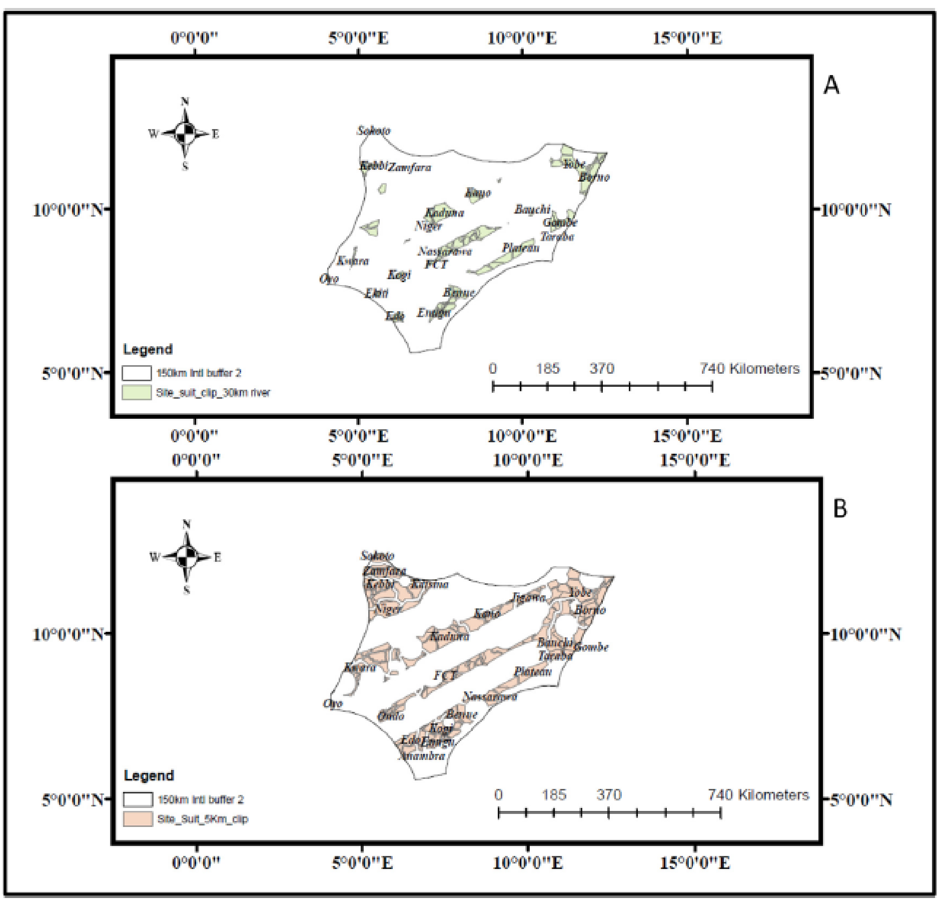

Figure 1. Map of suitable sites in Nigeria for NPP siting and other industrial construction using (A) criteria 1 (30 km proximity buffer on drainage (river) system of Nigeria) and (B) criteria 2 (5 km proximity buffer on drainage system of Nigeria).

Recuperado de: https://doi.org/10.1016/j.sciaf.2019.e00240

A planning-support tool for spatial suitability assessment of green urban stormwater infrastructure

Kuller, M., Bach, P., Roberts, S., Browne, D. and Deletic, A., (2019). *Science of the Total Enviroment,* 686, 856-868.

Abstract

Distributed green stormwater management infrastructure is increasingly applied worldwide to counter the negative impacts of urbanisation and climate change, while providing a range of benefits related to ecosystem services. They are known as Water Sensitive Urban Design (WSUD) in Australia, Nature Based Solutions (NBS) in Europe, Low Impact Development (LID) in the USA, and Sponge City systems in China. Urban planning for WSUD has been ad-hoc, lacking strategy and resulting in sub-optimal outcomes. The purpose of this study is to help improve strategic WSUD planning and placement through the development of a Planning Support System. This paper presents the development of Spatial Suitability ANalysis TOol (SSANTO), a rapid GIS-based Multi- Criteria Decision Analysis tool using a flexible mix of techniques to map suitability for WSUD assets across urban areas. SSANTO applies a novel WSUD suitability framework, which conceptualises spatial suitability for WSUD implementation from two perspectives: 'Needs' and 'Opportunities' for WSUD. It combines biophysical as well as socio-economic, planning and governance criteria ('Opportunities') with criteria relating to ecosystem services ('Needs'). Testing SSANTO through comparing its results to work done by a WSUD consultancy successfully verified its algorithms and demonstrated its capability to reflect and potentially enhance the outcomes of planning processes. Manual GIS based suitability analysis is time and resource intensive. Through its rapid suitability analysis, SSANTO facilitates iterative spatial analysis for exploration of scenarios and stakeholder.

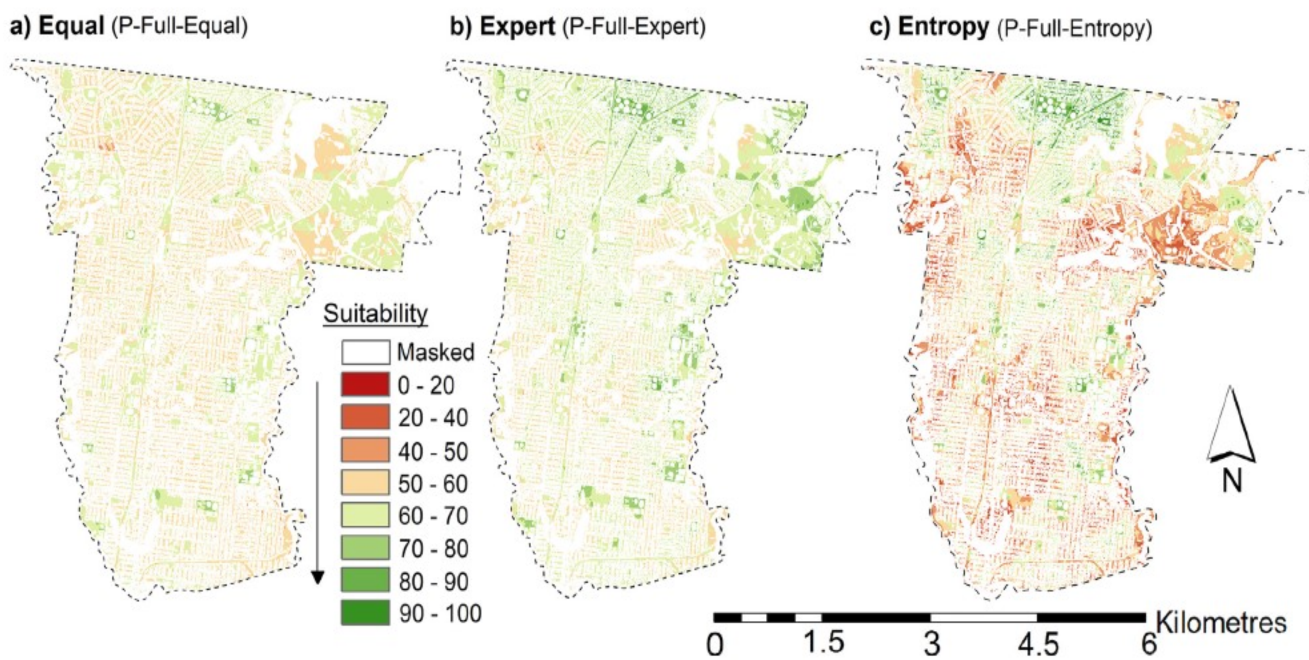

Figure 1. Comparing SSANTO results for different weighting methods for large systems using full criteria. a) Equal weights, b) expert weights, and c) entropy weights.

Recuperado de: https://doi.org/10.1016/j.scitotenv.2019.06.051

UNIVERSIDAD AUTÓNOMA DE SINALOA
FACULTAD DE CIENCIAS DE LA TIERRA Y EL ESPACIO

Applicability of GIS-based spatial interpolation and simulation for estimating the soil organic carbon storage in karst regions

Royal Belgian Institute of Natural Sciences, Operational Directorate Natural Environments, Vautierstraat 29, 1000, Brussels, Belgium (2020). *Remote Sensing of Enviroment,* 237.

Abstract

The applicability of the ordinary kriging method for estimating the soil organic carbon (SOC) stored in karst regions was investigated. A total of 23,536 soil samples were analysed from 2755 soil profiles collected using a grid-based sampling method in a typical small karst basin of western Guizhou in Southwest China. Corrections for the gravel content and rock exposure rate were applied to the GIS-based spatial interpolation and simulation and were compared with the same approach with the addition of soil profiles. With the addition of the soil profile data, the SOC stored in the karst catchment was accurately calculated as follows: 1.48 × 10^8 kg at a depth of 10 cm, 2.65 × 10^8 kg at 20 cm, 3.43 × 10^8 kg at 30 cm, and 5.39 × 10^8 kg at 100 cm. With the interpolation that was corrected for the rock exposure rate and soil depth, the resulting carbon storage estimation was 1.14e1.19 times higher than the most accurate estimate (that with the soil profiles), with an error rate of 114% - 119%. Since the conventional geostatistical method failed to accurately fit the data, including the spatial distribution, microgeomorphic features, rock exposure rate, and depth of the soil patches in the highly sloped exposed bedrock, must be used to correct the estimation of the SOC storage and organic carbon density in karst areas.

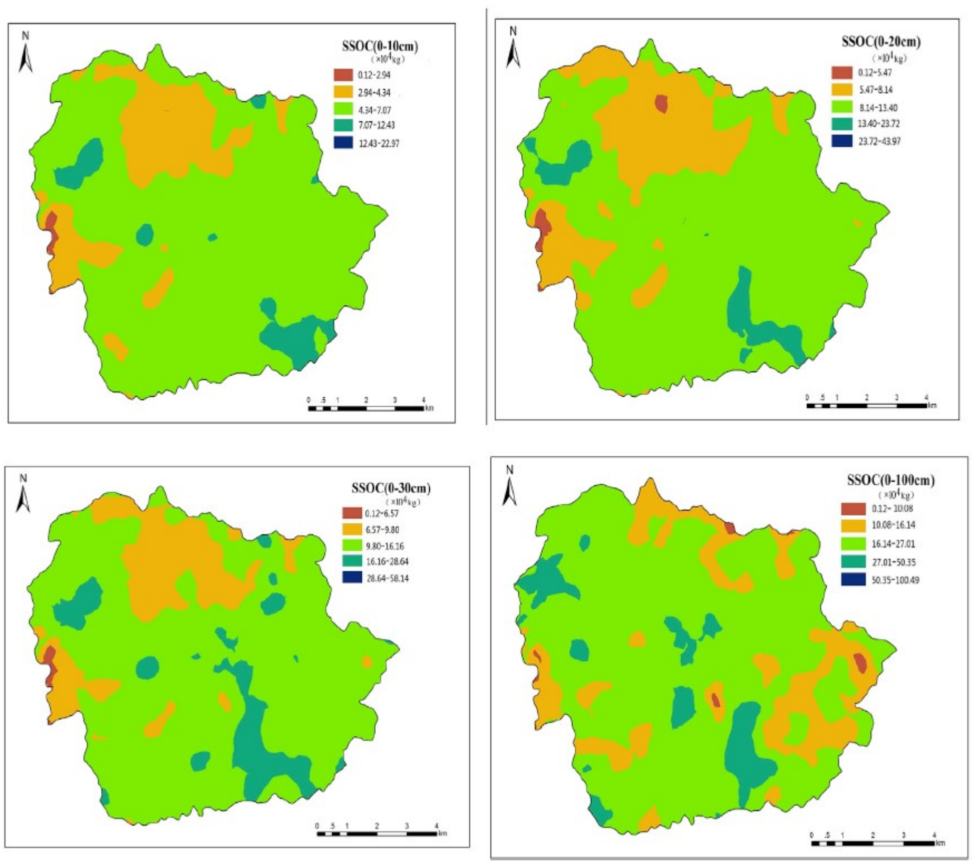

Figure 1. Spatial distribution of the soil organic carbon reserves in the Hou River basin based on a simulation created through GIS spatial interpolation.

Recuperado de: https://doi.org/10.1016/j.gecco.2019.e00849

UNIVERSIDAD AUTÓNOMA DE SINALOA
FACULTAD DE CIENCIAS DE LA TIERRA Y EL ESPACIO

Lenstool-HPC: A High Performance Computing based mass modelling tool for cluster-scale gravitational lenses

Schäfer, C., Fourestey, G. and Kneib, J., (2020). *Astronomy and Computing* , 30.

Abstract

With the upcoming generation of telescopes, cluster scale strong gravitational lenses will act as an increasingly relevant probe of cosmology and dark matter. The better resolved data produced by current and future facilities requires faster and more efficient lens modelling software. Consequently, we present Lenstool-HPC, a strong gravitational lens modelling and map generation tool based on High Performance Computing (HPC) techniques and the renowned Lenstool software. We also showcase the HPC concepts needed for astronomers to increase computation speed through massively parallel execution on supercomputers. Lenstool-HPC was developed using lens modelling algorithms with high amounts of parallelism. Each algorithm was implemented as a highly optimised CPU, GPU and Hybrid CPU–GPU version. The software was deployed and tested on the Piz Daint cluster of the Swiss National Supercomputing Centre (CSCS). Lenstool-HPC perfectly parallel lens map generation and derivative computation achieves a factor 30 speed-up using only 1 GPU compared to Lenstool. Lenstool-HPC hybrid Lens-model fit generation tested at Hubble Space Telescope precision is scalable up to 200 CPU–GPU nodes and is faster than Lenstool using only 4 CPU–GPU nodes.

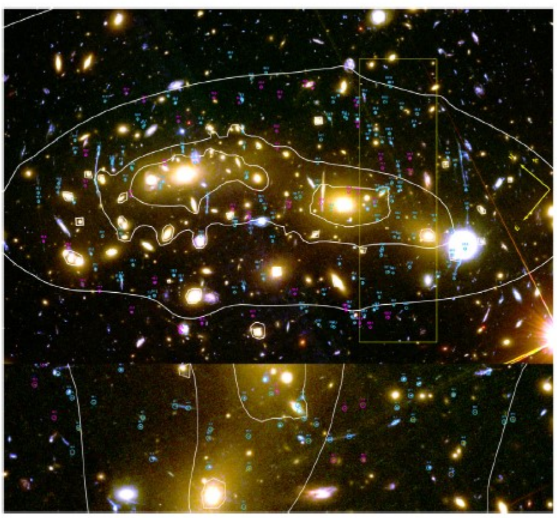

Figure 1. MACSJ0416-2403: The cluster has 68 confirmed multiple lensed background sources. The isolines trace the distribution of matter in the cluster which were computed using Lenstool. The highlighted (green) rectangle represents a zoomframe of the cluster showing the fainter multiple images. Credit. Jauzac et al. (2014).

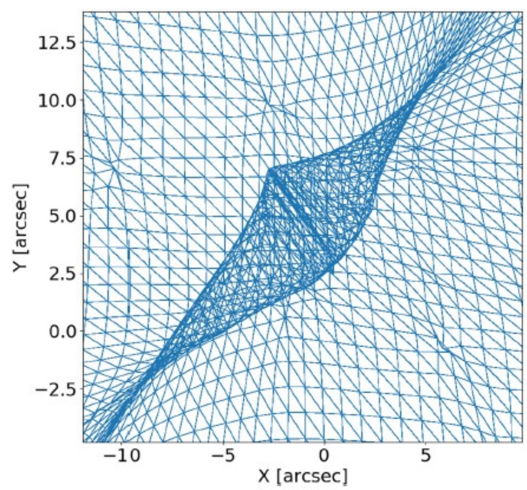

Figure 2. Graphical representation of the unlensing of the quadratic triangular grid from the image-plane unto the source plane. The lines which delimit the area where the grid folds unto itself (where therefore multiple images can be found) are the caustic lines.

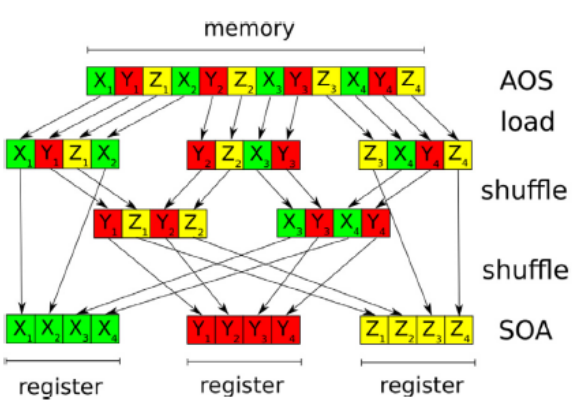

Figure 3. Preparation for vectorisation with a heterogeneous memory and AOS structures: The CPU core first loads from the main memory the needed information into AVX registers. Those registers have to be shuffled multiple times to achieve the needed homogeneous layout. Once the computations are done, they have to be reshuffled back into the AOS structure. Beyond the obvious time loss, the compiler is not able to vectorise these operations automatically. If developers still wish to implement AOS structures, SIMD pragmas have to be used to vectorise the operations manually. Xi, Yi and Zi represent fictional position information.

Recuperado de: ttps://doi.org/10.1016/j-nrjag.2018.07.006

UNIVERSIDAD AUTÓNOMA DE SINALOA
FACULTAD DE CIENCIAS DE LA TIERRA Y EL ESPACIO

An efficient parallel semi-implicit solver for anisotropic termal conduction in the solar corona

Ye, J., Shen, C, Lin, J. and Mei, Z., (2020). *Astronomy and Computing* , 30.

Abstract

Anisotropic thermal conduction plays an important role in determining the structure of the hot plasma in the solar corona. When hot plasma appears, the conductivity rises with temperature and becomes highly nonlinear. Explicit solvers for parabolic problems often lead to much smaller time-steps limited by a Courant–Friedrichs–Lewy (CFL) condition in comparison with hyperbolic Magnetohydrodynamics (MHD) equations. In this work, we present a pseudo-linear, directionally-split, semi-implicit method allowing for large time-steps as well as the optimized parallelization algorithm, integrated with the MHD solver. Our scheme can perfectly preserve the monotonicity and the geometry of shocks and discontinuities in complex MHD problems. Two sets of numerical tests show that an increase in time step of □ 600 can be easily achieved with an acceptable error by our scheme compared to explicit methods, and the use of large time-steps can still follow fast dynamic processes reliably. In addition, the extendibility studies have proven that the associated parallel efficiency is comparably high. This method is also useful for any kind of time-dependent conductivity problems for the solar applications in the future.

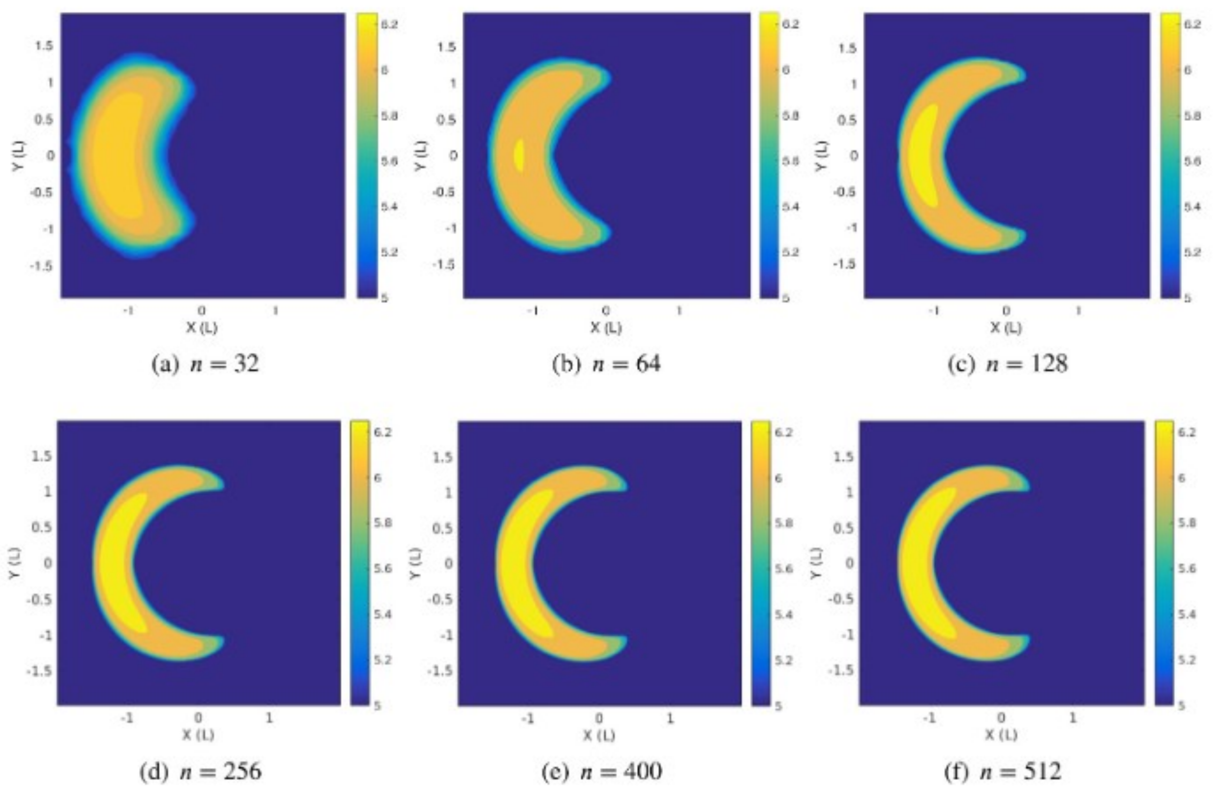

Figure 1. Log10 temperature contour plots at t = 3000 s for evaluating only the anisotropic diffusion scheme using a 128 × 128 grid. Different CFL numbers C were used to yield the Δt in Eqs. (12) and (13). Additionally, the temperature plot with fully explicit method is given for comparison.

Recuperado de: https://doi.org/10.1016/j.ascom.2019.03.002

Universidad Autónoma de Sinaloa
Facultad de Ciencias de la Tierra y el Espacio

NOTICIAS

El volcán más grande del mundo

Aunque parezca mentira, hasta hace relativamente poco tiempo los geólogos no tenían claro cuál era el volcán más grande del mundo. Después de una investigación sobre las características del monte Tamu, un volcán submarino apagado y situado en el océano Pacífico, considerado el mayor de la Tierra hasta ahora, y que determinó sus dimensiones con exactitud, los científicos concluyeron en julio de 2019 que el Mauna Loa es, en realidad, el volcán más grande del mundo.

El Mauna Loa es un volcán situado en la isla de Hawái, también en el Pacífico. A diferencia del Tamu, es un volcán en escudo que se halla activo, cuyo volumen y superficie lo sitúan en lo más alto del ranking mundial para estas estructuras geológicas.

Como en el resto de las islas hawaianas, el Mauna Loa y los otros volcanes de la región aparecieron primero como volcanes submarinos hace unos 700.000 años.

Noticia completa en: https://noticiasdelaciencia.com/art/36114/el-volcan-mas-grande-del-mundo

Consecuencias de los impactos cósmicos en la Tierra

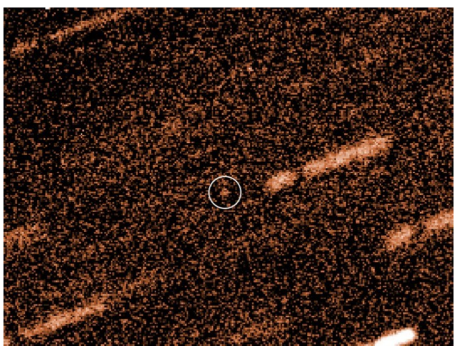

El choque de la Tierra contra un asteroide o cometa errante es quizá el posible episodio catastrófico más conocido. Esto no es extraño, puesto que ya ha ocurrido en el pasado, siendo uno de los más frecuentes en la Historia.

Nuestro mundo y el resto de los planetas evolucionan en órbitas estables y tranquilas alrededor de nuestra estrella, pero el Sistema Solar contiene también una considerable población de residuos procedentes de su época de formación, o como resultado de colisiones, que en ocasiones pululan demasiado cerca de nosotros y pueden producir impactos cósmicos.

Los más peligrosos componentes de esta facción son aquellos que cruzan la órbita de la Tierra. El primero se descubrió hace 60 años y desde entonces no han dejado de aparecer nuevos candidatos para protagonizar un encuentro mortal. En realidad, no son muchos, ya que la mayor parte de los objetos que podían haber chocado contra la Tierra ya lo han hecho durante la larga historia del sistema planetario (como prueba la craterizada faz de la Luna).

Noticia completa en: https://noticiasdelaciencia.com/art/36157/consecuencias-de-los-impactos-cosmicos-en-la-tierra

Nueva tecnología para la detección de eventos sísmicos submarinos

Un equipo internacional de científicos de la Universidad de Alcalá (España) y el Instituto Tecnológico de California (Caltech) acaba de publicar en la revista 'Nature Communications', el estudio 'Detección distribuida de microseismos y teleseismos empleando fibra oscura submarina', un trabajo que recoge los resultados de las pruebas que han llevado a cabo en el fondo del Mar del Norte. En ellas, han utilizado cables de comunicaciones de fibra óptica instalados a modo de una red sísmica gigante, con el fin de rastrear terremotos lejanos y olas oceánicas.

El proyecto fue, en parte, una prueba de concepto de una nueva tecnología desarrollada por la Universidad de Alcalá para la medida de eventos sísmicos. Los océanos cubren dos tercios de la superficie terrestre, pero colocar sismómetros permanentes bajo el mar es prohibitivamente caro. El grupo de la UAH ha desarrollado un nuevo sensor multipunto de eventos sísmicos empleando solamente cables de fibra óptica convencionales de comunicaciones, que son cada vez más comunes en el fondo del mar. Basta con conectar un equipo en el extremo de tierra de estos cables, y esta tecnología permite transformarlo en una potente matriz de sensores sísmicos.

Noticia completa en: https://noticiasdelaciencia.com/art/35914/nueva-tecnologia-para-la-deteccion-de-eventos-sismicos-submarinos

UNIVERSIDAD AUTÓNOMA DE SINALOA
FACULTAD DE CIENCIAS DE LA TIERRA Y EL ESPACIO

CONGRESOS

XI Congreso Internacional Geomática 2020

Sede: La Habana, Cuba

Fecha: 16 al 20 de marzo del 2020

Más información en: http://www.nosolosig.com/geo-eventos/1093-xi-congreso-internacional-de-geomatica-2020

II Congreso Internacional del Desarrollo Territorial

Sede: Durango, México

Fecha: 1, 2 y 3 de abril del 2020